

DETECTING THE COMPANIONS AND ELLIPSOIDAL VARIATIONS OF RS CVN PRIMARIES: II. *o* DRACONIS, A CANDIDATE FOR RECENT LOW-MASS COMPANION INGESTION

RACHAEL M. ROETTENBACHER¹, JOHN D. MONNIER¹, FRANCIS C. FEKEL², GREGORY W. HENRY², HEIDI KORHONEN³,
DAVID W. LATHAM⁴, MATTHEW W. MUTERSPAUGH², MICHAEL H. WILLIAMSON², FABIEN BARON¹,
THEO A. TEN BRUMMELAAR⁵, XIAO CHE¹, ROBERT O. HARMON⁶, GAIL H. SCHAEFER⁵, NICHOLAS J. SCOTT⁵,
JUDIT STURMANN⁵, LASZLO STURMANN⁵, AND NILS H. TURNER⁵

¹Department of Astronomy, University of Michigan, Ann Arbor, MI 48109, USA

²Center of Excellence in Information Systems, Tennessee State University, Nashville, TN 37209, USA

³Finnish Centre for Astronomy with ESO (FINCA), University of Turku, Väisäläntie 20, FI-21500 Piikkiö, Finland

⁴Harvard-Smithsonian Center for Astrophysics, 60 Garden Street, Cambridge, MA 02138, USA

⁵Center for High Angular Resolution Astronomy, Georgia State University, Mount Wilson, CA 91023, USA

⁶Department of Physics and Astronomy, Ohio Wesleyan University, Delaware, OH 43015, USA

Accepted for publication in the Astrophysical Journal

ABSTRACT

To measure the stellar and orbital properties of the metal-poor RS CVn binary *o* Draconis (*o* Dra), we directly detect the companion using interferometric observations obtained with the Michigan InfraRed Combiner at Georgia State University's Center for High Angular Resolution Astronomy (CHARA) Array. The *H*-band flux ratio between the primary and secondary stars is the highest confirmed flux ratio (370 ± 40) observed with long-baseline optical interferometry. These detections are combined with radial velocity data of both the primary and secondary stars, including new data obtained with the Tillinghast Reflector Echelle Spectrograph on the Tillinghast Reflector at the Fred Lawrence Whipple Observatory and the 2-m Tennessee State University Automated Spectroscopic Telescope at Fairborn Observatory. We determine an orbit from which we find model-independent masses and ages of the components ($M_A = 1.35 \pm 0.05 M_\odot$, $M_B = 0.99 \pm 0.02 M_\odot$, system age = 3.0 ∓ 0.5 Gyr). An average of a 23-year light curve of *o* Dra from the Tennessee State University Automated Photometric Telescope folded over the orbital period newly reveals eclipses and the quasi-sinusoidal signature of ellipsoidal variations. The modeled light curve for our system's stellar and orbital parameters confirm these ellipsoidal variations due to the primary star partially filling its Roche lobe potential, suggesting most of the photometric variations are not due to stellar activity (starspots). Measuring gravity darkening from the average light curve gives a best-fit of $\beta = 0.07 \pm 0.03$, a value consistent with conventional theory for convective envelope stars. The primary star also exhibits an anomalously short rotation period, which, when taken with other system parameters, suggests the star likely engulfed a low-mass companion that had recently spun-up the star.

Subject headings: binaries: close – stars: activity – stars: imaging – stars: individual (*o* Draconis) – stars: variables: general

1. INTRODUCTION

RS Canum Venaticorum (RS CVn) stars are active binary systems with Ca H and K and photometric variability (Hall 1976). The components of these close binary systems are typically an evolved giant or subgiant primary star with a subgiant or main sequence companion (Berdyugina 2005; Strassmeier 2009).

In close binary systems, the stars experience changes in energy and angular momentum, circularizing the orbit due to forces from the aspherical mass distributions of the (partially) Roche-lobe-filling primary stars (Zahn 1977). Observations of open clusters have shown a transition period, the range of orbital periods between the longest circular orbit and the shortest eccentric orbit, which monotonically increases with cluster age (Mazeh 2008, and references therein). Observations and predictions have shown that stars with orbital periods $P_{\text{orb}} \lesssim 10$ days will have circularized while on the main sequence, regardless of spectral type (e.g., Walter 1949; Koch & Hrivnak 1981; Zahn & Bouchet 1989). As stars evolve off of the

main sequence and cool while becoming subgiants and giants, circularization is expected for stars with periods $P_{\text{orb}} \lesssim 100$ days (e.g., Mayor & Mermilliod 1984; Claret 2009). Therefore, RS CVn systems with orbital periods longer than 100 days are likely to retain primordial non-zero eccentricities.

The single-lined RS CVn system *o* Draconis (omicron Draconis, *o* Dra, 47 Dra, HD 175306, HIP 92512, HR 7125; G9III; Herbig & Spalding 1955; Young & Koniges 1977; Walter 1985; Strassmeier et al. 1989) has a previously-measured orbital period of $P_{\text{orb}} \sim 138$ days with a non-zero eccentricity of $e \sim 0.1$ (e.g., Young 1921; Lucy & Sweeney 1971; Massarotti et al. 2008). The primary star of *o* Dra rotates faster than would be expected from tidal synchronization (e.g. Głębocki & Stawikowski 1988; Massarotti et al. 2008).

To achieve this rapid rotation, the primary star must have increased its angular momentum. One possibility is that the primary star engulfed a nearby companion, an event that would have had a strong impact on the primary star and its subsequent evolu-

tion. This evolution could shed light on the future of the Solar System as the Sun expands to ingest planets (e.g., Schröder & Connors 2008). To investigate this hypothesis, we aim to better determine *o* Dra’s stellar parameters (e.g., Basri et al. 1985; Gurzadyan & Cholakyan 1995) and thereby resolve the binary system’s history.

To advance our understanding of *o* Dra, we present the first detections of the low luminosity companion with six nights of interferometric data and the companion’s first radial velocity detections. We describe these data sets along with radial velocity and photometric data of the primary star in Section 2. We detail the analysis of observations with resultant orbital parameters in Section 3. We describe the analysis of our photometry, show the detected ellipsoidal variations and eclipses, and measure gravity darkening of the primary component in Section 4. We show our results on an Hertzsprung-Russell (H-R) diagram and discuss the system’s evolution in Section 5. Finally, we present the conclusions of our study of *o* Dra in Section 6.

2. OBSERVATIONS

2.1. Interferometry

We obtained interferometric data at Georgia State University’s Center for High-Angular Resolution Astronomy (CHARA) Array. The CHARA Array is a Y-shaped array of six 1-m class telescopes with non-redundant baselines varying from 34- to 331-m located at Mount Wilson Observatory, California (ten Brummelaar et al. 2005). Using all six telescopes and the Michigan InfraRed Combiner (MIRC; Monnier et al. 2004, 2006; Che et al. 2011), we obtained *H*-band (1.5 – 1.8 μm) data (eight channels across the photometric band with $\lambda/\Delta\lambda \sim 40$) on UT 2012 May 9, 11, 12 and June 6, 8, 17, 18; 2014 May 25, 26, 27, June 29, 30, and July 1.

We detected the faint companion in the data from UT 2012 May 9, 12; 2012 June 17, 18; and 2014 May 26, 27. The nights of observation without detections of the companion had insufficient *uv* coverage due to poor seeing, short observation lengths, or observations during eclipse leaving the companion undetected. We reduced and calibrated these data with the standard MIRC pipeline (see Monnier et al. 2007; Zhao et al. 2009; Monnier et al. 2012, for pipeline details). We used at least two calibration stars for each night of data (see Table 1).

Three of our seven calibrators are A stars, which were revealed to be oblate due to rapid rotation during our analysis and required more information for calibration. Each of the stars were calibrated with a non-oblate star when possible, but some nights of observation required the use of other oblate stars. HD 185395 (θ Cyg) was used on 2012 Jun 17 to calibrate HD 192696 (33 Cyg) and HD 184006 (ι Cyg). On nights when HD 185395 was not available (2012 Jun 8 and 18), HD 192696 and HD 184006 were used to calibrate each other. HD 192696 was used to calibrate HD 106591 (δ UMa) on 2012 May 9, 11, and 12). The calibrated visibilities were fit to models of oblate stars to determine the mean uniform disk diameter, major-to-minor axis ratio, and position angle of the major axis (east of north), the mean values of which are in the footnotes of Table 1.

2.2. Radial Velocity

We combined three radial velocity data sets of the primary star and one set for the secondary to further constrain our orbit of *o* Dra.

Three radial velocities published in Massarotti et al. (2008) were obtained with the CfA Digital Speedometer on the Wyeth Reflector at the Oak Ridge Observatory (Harvard, MA; 2004 September 1– 2005 April 14). Two radial velocities also published in Massarotti et al. (2008) were obtained with the CfA Digital Speedometer on the Tillinghast Reflector at the Fred L. Whipple Observatory (Mount Hopkins, AZ; 2006 June 14 – 2007 September 21). Six additional radial velocities (2012 May 9 – 2012 October 10) for the primary star were taken with the Tillinghast Reflector Echelle Spectrograph (TRES) at the Tillinghast Reflector (see Table 2).

With the Tennessee State University 2-m automatic spectroscopic telescope (AST) at Fairborn Observatory, AZ, we have determined radial velocities from 86 spectrograms of the primary of *o* Dra taken between 2007 October 11 – 2014 October 28 and 19 measurements of the companion radial velocity (2012 October 10 – 2014 October 28; see Table 3). See Appendix A, Fekel et al. (2009), and Roettenbacher et al. (2015) for details on these observations.

We additionally include 18 archival radial velocities of the primary star from Young (1921, 1902 July 15 – 1920 August 9).

2.3. Photometry

o Dra has been monitored since 1992 with Tennessee State University’s T3 0.4-m Automatic Photometric Telescope (APT) at Fairborn Observatory. Our observations span over 23 years from 1992 March 24 – 2015 May 13, but with a gap during 2005–2011 (see Table 4 and Figure 1). Our Johnson *B* and *V* measurements of *o* Dra were made differentially with respect to the comparison star HD 175511 (HIP 92594; B9; see Figure 2) and the check star HD 176408 (K1III). Details of the robotic telescopes and photometers, observing procedures, and data analysis techniques can be found in Henry (1999) and Fekel et al. (2005).

2.4. High-Resolution Spectroscopy

We use high-resolution spectra of *o* Dra covering the spectral range of 3700 – 7300 \AA obtained at the Nordic Optical Telescope (NOT) with the FIES high resolution echelle spectrograph. In the current work, the 1.3 arc-sec fiber giving a resolving power ($\lambda/\Delta\lambda$) of 67000 was used. The exposure time for each spectrum was 180 s and resulted in a typical signal-to-noise ratio of 500 per resolution element (four pixels) at 6420 \AA . The observations were carried out at thirteen epochs between 2012 April 17 – August 15. All the spectra were reduced with the dedicated FIES reduction software FIESStool.

3. ORBITAL ELEMENTS AND MASSES

Using model fitting for the location of the unresolved secondary star with respect to the resolved primary star, we directly detected the companion of *o* Dra. Our models allow the primary star’s major axis and major-to-minor axis ratio, primary-to-secondary *H*-band flux ratio, and the secondary’s position to vary. During the fitting for

TABLE 1
CALIBRATORS FOR *o* DRACONIS

Calibrator Name	Calibrator Size (mas) ^a	Source	UT Date of Observation
HD 106591 (δ UMa)	oblate ^b	MIRC calibration	2012 May 9, 12
HD 125161 (ι Boo)	0.49 ± 0.03	Bonneau et al. (2006)	2012 May 9, 12
HD 138852	1.00 ± 0.06	Bonneau et al. (2006)	2014 May 26
HD 184006 (ι Cyg)	oblate ^c	MIRC calibration	2012 Jun 17, 18; 2014 May 26, 27
HD 185264	0.80 ± 0.06	Bonneau et al. (2006)	2014 May 26, 27
HD 185395 (θ Cyg)	0.73 ± 0.02	White et al. (2013)	2012 Jun 17
HD 192696 (33 Cyg)	oblate ^d	MIRC calibration	2012 May 9, 12, Jun 17, 18

NOTE. — ^a Some calibration stars are rapidly rotating and distorted from spherical. They were modeled as *H*-band uniform ellipses for calibration. For each star we list the *H*-band uniform disk mean diameter (mas), major-to-minor axis ratio, and position angle of the major axis ($^\circ$, east of north).

^b $\theta_{\text{UD,mean}} = 0.78 \pm 0.02$, major/minor = 1.29 ± 0.05 , $\text{PA}_{\text{maj}} = 113 \pm 5^\circ$

^c $\theta_{\text{UD,mean}} = 0.72 \pm 0.02$, major/minor = 1.29 ± 0.04 , $\text{PA}_{\text{maj}} = 92 \pm 4^\circ$

^d $\theta_{\text{UD,mean}} = 0.56 \pm 0.02$, major/minor = 1.41 ± 0.09 , $\text{PA}_{\text{maj}} = 115 \pm 6^\circ$

TABLE 2
RADIAL VELOCITY DATA OF
o DRACONIS (WYETH &
TILLINGHAST/CFA)

HJD -2400000	Primary (km s ⁻¹)
53249.7015	-27.27
53306.5778	-31.61
53474.7086	4.10
53900.9303	2.21
54364.6628	-31.30
56056.9907	-42.65
56075.9832	-30.30
56110.9890	3.86
56132.6637	-6.89
56198.7292	-41.88
56210.5694	-34.50

NOTE. — Residuals on the primary radial velocities are 0.39 km s^{-1} . The first five velocities are published in Massarotti et al. (2008).

TABLE 3
RADIAL VELOCITY DATA OF *o* DRACONIS (AST/TSU)

HJD -2400000	Primary (km s ⁻¹)	Secondary (km s ⁻¹)
54384.710	-41.9	
56210.620	-34.5	-1.2
56211.589	-33.4	
56212.589	-32.6	
56227.713	-12.2	

NOTE. — Table 3 is published in its entirety in the electronic edition. Residuals on the primary radial velocities are 0.22 km s^{-1} and secondary are 1.6 km s^{-1} .

the companion we weighted the closure phases ten times more strongly in the final χ^2 than the squared visibilities and triple amplitudes in order to better identify asymmetries in the system to detect the faint companion (the detection of the companion is not sensitive to the factor of 10; see Figures 10 – 13 in Appendix B). Errors for the primary star's size and shape and the primary-to-secondary *H*-band flux ratio are based on the individual epochs. The positional errors of the location of the secondary are error ellipses based upon the shape of the χ^2 surface used to detect the companion.

The coordinates of the secondary detections on six nights (UT 2012 May 9, 12; June 17, 18; 2014 May 26 and 27) are listed in Table 5. We measured the *H*-

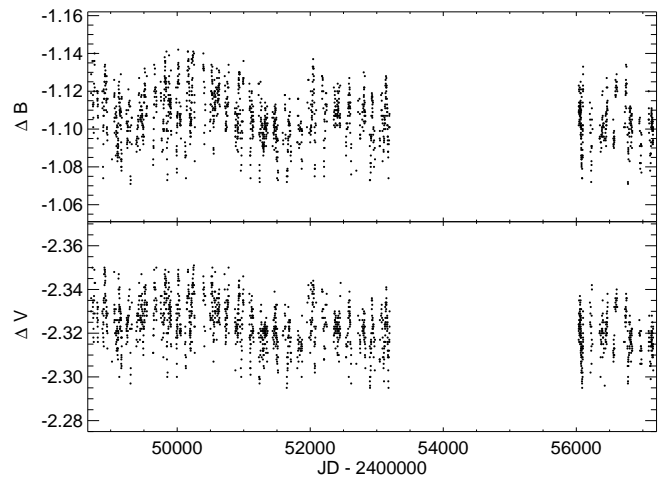


FIG. 1.— Johnson *B* and *V* differential magnitudes of *o* Dra acquired over 23 years from 1992 – 2015 with the T3 0.4-meter APT at Fairborn Observatory in southern Arizona.

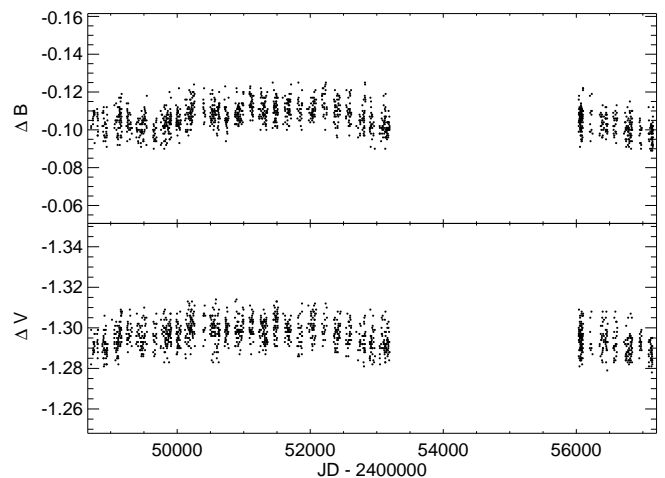


FIG. 2.— Johnson *B* and *V* differential magnitudes of comparison star HD 175511 (with the check star 48 Dra).

band uniform disk diameter of the primary star to be $\theta_{\text{UD}} = 2.115 \pm 0.007 \text{ mas}$ (limb-darkened disk $\theta_{\text{LD}} = 2.189 \pm 0.007$, obtained by assuming a limb darkening power law exponent $\alpha = 0.27$) with a major-to-minor

TABLE 4
DIFFERENTIAL JOHNSON B AND V PHOTOMETRIC DATA OF α DRACONIS (APT/TSU)

HJD-2400000	ΔB (α Dra - HD 175511)	ΔV (α Dra - HD 175511)	ΔB (48 Dra ^a - HD 175511)	ΔV (48 Dra - HD 175511)
48705.9454	-1.119	-2.330	-0.101	-1.282
48706.9415	-1.129	-2.336	-0.102	-1.299
48725.8916	-1.136	-2.350		
48732.8732	-1.113	-2.332	-0.106	
48733.8831	-1.118	-2.334	-0.105	-1.287

NOTE. — Table 4 is published in its entirety in the electronic edition.

^a HD 175511 (HIP 92594), $V = 6.94$, $B - V = -0.04$.

^b 48 Dra (HD 176408, HIP 92997), $V = 5.68$, $B - V = 1.16$.

axis ratio of 1.01 ± 0.03 . The H -band flux ratio for the primary star to the secondary is 370 ± 40 , the highest confirmed binary flux ratio measured with long-baseline optical interferometry (RT Aur has an unconfirmed H -band flux ratio of $\sim 450:1$, measured by MIRC at the CHARA Array; Gallenne et al. 2015).

We calculate the orbital parameters of the binary by simultaneously fitting our interferometric and radial velocity data with Monte Carlo realizations. For our six interferometric points we present the error ellipses of the major and minor axis in Table 5 scaled to give our fit a reduced $\chi^2 = 1.00$. The radial velocity errors are similarly scaled to require $\chi^2 = 1.00$ ($\text{rms}_{\text{CF},A} = 0.39 \text{ km s}^{-1}$, $\text{rms}_{\text{AST},A} = 0.22 \text{ km s}^{-1}$, $\text{rms}_{\text{AST},B} = 1.6 \text{ km s}^{-1}$, $\text{rms}_{\text{Young},A} = 2.2 \text{ km s}^{-1}$).

The simultaneous radial velocity and astrometry Monte Carlo realizations of the orbit gave the orbital parameters and their $1 - \sigma$ errors listed in Table 6. The orbit is represented in Figure 3 with the radial velocity curve in Figure 4. We use the conventions presented by Heintz (1978), where the argument of periastron, ω , follows the radial velocity orbit convention (the primary star with respect to the center of mass), which is different from the visual orbit convention (the secondary star with respect to the primary). The position angle of the ascending node (E of N), Ω , is independent of definition being equivalent with respect to either the primary or secondary star.

Our double-lined and visual orbit confirms previous analyses of orbital period and non-zero eccentricity (e.g., Young 1921; Lucy & Sweeney 1971), while highlighting new evidence that the system is eclipsing ($i = 89.6 \pm 0.3^\circ$). We determine the masses of the stars to be $M_A = 1.35 \pm 0.05 M_\odot$ and $M_B = 0.99 \pm 0.02 M_\odot$; the implications to system evolution will be discussed in Section 5. Our orbit gives a parallax of $\pi = 9.36 \pm 0.10 \text{ mas}$, a value consistent with van Leeuwen (2007, $\pi = 9.54 \pm 0.21 \text{ mas}$) but about $2 - \sigma$ from the original Hipparcos reduction ($\pi = 10.12 \pm 0.43 \text{ mas}$; ESA 1997), confirmed by Pourbaix & Boffin (2003, $\pi = 10.27 \pm 0.42 \text{ mas}$). Adopting the spectroscopic orbit presented here, the resulting Hipparcos parallax becomes $\pi = 10.15 \pm 0.43 \text{ mas}$ (Pourbaix, private communication). The origin of the $2 - \sigma$ discrepancy in parallax measurements is not well-understood; for our purposes in later sections, we proceed with our derived value of $\pi = 9.36 \pm 0.10 \text{ mas}$.

4. LIGHT CURVE MODELS AND ELLIPSOIDAL VARIATIONS

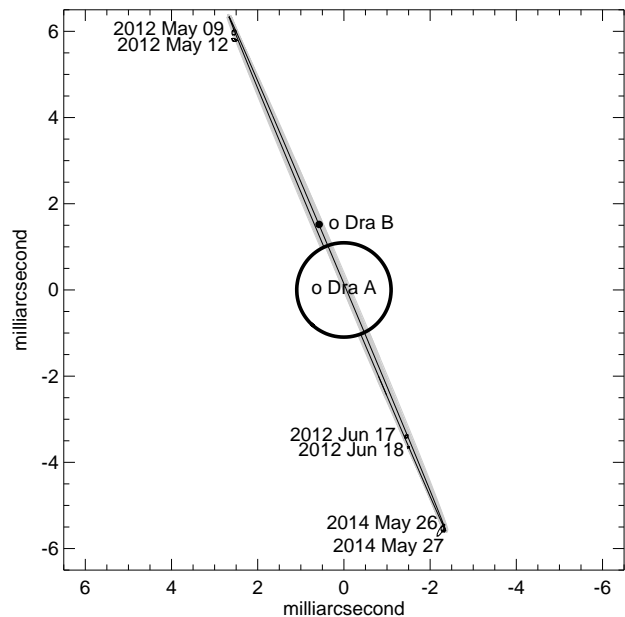


FIG. 3.— Visual orbit of the RS CVn system α Dra with our dates of companion detection and their locations on the orbit (black error ellipses). The observed stellar radius of the primary star is plotted with a thick black line (α Dra A). The radius of the companion star, α Dra B, for the best-fit temperature of 6000 K is plotted as the small black circle. The light gray orbits represent fifty Monte Carlo realizations. Black lines connect the center of the detection error ellipse to the expected point in the best-fit orbit, which is overlaid in black (given in Table 6 with $1 - \sigma$ errors). At the southernmost point in the orbit, the secondary star is moving toward the observer. Note: the axis units are milliarcseconds (mas) with north upwards and east to the left.

A previous study, Strassmeier et al. (1989), suggested α Dra has photometric variations up to $\Delta V \sim 0.01 \text{ mag}$. Other indications of activity include chromospheric Ca H and K emission and variation (Young & Koniges 1977; Simon & Fekel 1987; Strassmeier et al. 1988). Hall & Persinger (1986) reported a possible rotation period of $P_{\text{rot}} = 54.6 \text{ days}$ from photometric observations. Using our NOT spectra, we can determine the value of $v \sin i$. We modeled the Fe 6421 Å line with a variety of $v \sin i$ models from Castelli & Kurucz (2004) with $T_{\text{eff},A} = 4530 \text{ K}$, $\log g_A = 1.77$, $[\text{Fe}/\text{H}] = -0.5$, microturbulence $\xi_m = 1.4 \text{ km s}^{-1}$, and macroturbulence $\xi_M = 6 \text{ km s}^{-1}$. The resultant value is $v \sin i = 16 \pm 0.5 \text{ km s}^{-1}$ when combined with our observed pri-

TABLE 5
DETECTIONS FOR THE COMPANION OF *o* DRACONIS WITH RESPECT TO THE PRIMARY

UT Date	JD -2400000	Separation (mas)	Position ($^{\circ}$) ^a	Error Ellipse Major Axis (mas) ^b	Error Ellipse Minor Axis (mas) ^b	Error Ellipse Position Angle ($^{\circ}$) ^a	Reduced χ^2
2012 May 09	56056.97	6.52	23.1	0.06	0.04	340	1.3
2012 May 12	56059.95	6.36	23.7	0.05	0.03	60	1.5
2012 June 17	56095.87	3.71	203.1	0.04	0.03	310	1.6
2012 June 18	56096.82	3.96	202.3	0.02	0.02	330	1.5
2014 May 26	56803.87	6.03	202.5	0.07	0.05	20	0.9
2014 May 27	56804.85	6.04	202.0	0.16	0.04	330	1.1

NOTE. — These detections give an *H*-band (1.5 – 1.8 μ m) primary-to-secondary flux ratio for *o* Dra A to B of 370 ± 40 . The uniform disk fit for the primary star is 2.115 ± 0.007 mas (limb-darkened disk 2.189 ± 0.007) with a 1.01 ± 0.03 major-to-minor axis ratio.

^aEast of North

^bScaled error bars to ensure a reduced $\chi^2 = 1.00$ as described in Section 3.

TABLE 6
ORBITAL AND STELLAR PARAMETERS OF *o* DRACONIS

Measured Parameters	Value
semi-major axis, a (mas)	6.51 ± 0.03
eccentricity, e	0.158 ± 0.003
inclination, i ($^{\circ}$)	89.6 ± 0.3
argument of periastron, ω ($^{\circ}$) ^a	293.0 ± 0.6
ascending node, Ω ($^{\circ}$, E of N)	22.9 ± 0.2
period, P_{orb} (days)	138.444 ± 0.003
time of periastron passage, T (HJD)	2454983.0 ± 0.2
velocity semi-amplitude, K_A (km s $^{-1}$)	23.42 ± 0.05
velocity semi-amplitude, K_B (km s $^{-1}$)	32.0 ± 0.4
system velocity, γ (km s $^{-1}$)	-20.77 ± 0.04
<i>H</i> -band uniform disk diameter, $\theta_{\text{UD},A}$ (mas)	2.115 ± 0.007
<i>H</i> -band limb-darkened disk diameter, $\theta_{\text{LD},A}$ (mas) ^b	2.189 ± 0.007
primary major-to-minor axis ratio	1.01 ± 0.03
<i>B</i> -band flux ratio, primary-to-secondary	60 ± 20
<i>V</i> -band flux ratio, primary-to-secondary	130 ± 80
<i>H</i> -band flux ratio, primary-to-secondary	370 ± 40
rotational velocity, $v \sin i$ (km s $^{-1}$)	16.0 ± 0.5
Derived Parameters	
orbital parallax, π (mas)	9.36 ± 0.10
distance, d (pc)	106.8 ± 1.1
primary radius, R_A (R_{\odot}) ^c	25.1 ± 0.3
primary luminosity, L_A (L_{\odot})	220 ± 30
primary surface gravity, $\log g_A$ (cm/s 2)	1.769 ± 0.007
primary mass, M_A (M_{\odot})	1.35 ± 0.05
primary rotation period, P_{rot} (days) ^d	79 ± 3
secondary radius, R_B (R_{\odot})	1.0 ± 0.1
secondary luminosity, L_B (L_{\odot})	1.3 ± 0.2
secondary surface gravity, $\log g_B$ (cm/s 2)	4.43 ± 0.09
secondary mass, M_B (M_{\odot})	0.99 ± 0.02
secondary temperature, $T_{\text{eff},B}$ (K)	6000^{+400}_{-300}
system age (Gyr)	3.0 ∓ 0.5
Literature Parameters	
primary effective temperature, $T_{\text{eff},A}$ (K) ^e	4430 ± 130
primary metallicity, Fe/H ^f	-0.5

NOTE. — ^aRadial velocity convention for primary with respect to the center of mass.

^bWe applied a 3.5% correction from uniform to limb-darkened disk diameter, which is consistent with a limb-darkening power law exponent of $\alpha = 0.27$.

^cUsing limb-darkened disk diameter.

^dAssuming $i_{\text{rot}} = i_{\text{orb}}$.

^e $T_{\text{eff},A}$ is an average of temperatures given by Christian & Janes (1977); Głębcki & Stawikowski (1977); Rutter & Schrijver (1987); Głębcki & Stawikowski (1988); McWilliam (1990); Luck (1991); Pourbaix & Boffin (2003); Böhm-Vitense (2004); Massarotti et al. (2008); Soubiran et al. (2010); McDonald et al. (2012). The $1 - \sigma$ error is the standard deviation of these values.

^f[Fe/H] is approximated in stellar evolution models based upon values given by McWilliam (1990); Massarotti et al. (2008); Soubiran et al. (2010).

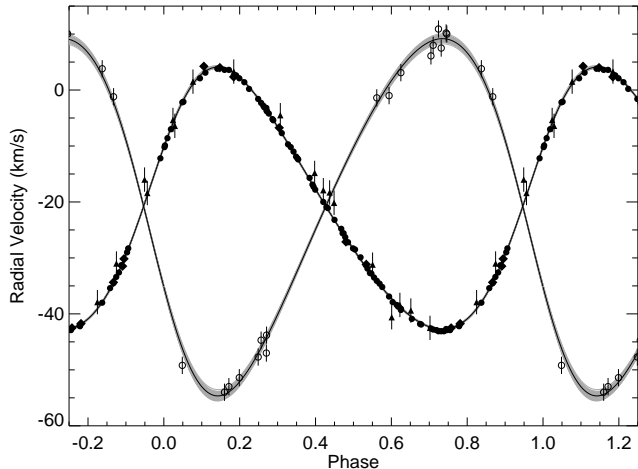


FIG. 4.— Radial velocity curves of the components of *o* Dra. The filled symbols represent measurements of the primary star. The filled diamonds represent observations from Massarotti et al. (2008)/CfA. The filled circles are the AST observations. The filled triangles are observations from Young (1921). $1 - \sigma$ errors in velocity are plotted unless the error is smaller than the symbols. Similarly, the open circles represent AST radial velocity data for the secondary star with $1 - \sigma$ error bars. The gray orbits are fifty Monte Carlo realizations (dark gray for the primary star and light gray for the secondary star) with the best-fit orbital parameters overlaid in black. See Table 6 for orbital parameters with $1 - \sigma$ errors.

primary radius and orbital inclination (assuming $i_{\text{orb}} = i_{\text{rot}}$) gives $P_{\text{rot},A} = 79 \pm 3$ days.

We investigate the APT Johnson *B* and *V* differential light curves for evidence of starspots. We removed long-term variations ($\Delta V \sim 0.02$) that may be attributed to axisymmetric spot structures or polar spot structures. We folded the adjusted light curves over the orbital period ($P_{\text{orb}} = 138.444$ days) and binned the data (0.01 in phase). The resultant Johnson *B* and *V* light curves are presented in Figure 5. The quasi-sinusoidal trend observed in the averaged light curves suggests ellipsoidal variations due to distortions of the primary star partially filling its Roche lobe potential ($R_L = 60.8 R_\odot$, $R_A/R_L = 0.42$; e.g., Roettenbacher et al. 2015). Both light curves clearly show an eclipse (phase ~ 0.95) and evidence of a weak eclipse (phase ~ 0.40). Comparing the timing of the eclipses to the radial velocity curve and visual orbit, we see that the deeper eclipse is associated with the secondary star moving behind the primary star, revealing that the secondary star is hotter than the primary star.

The secondary eclipse provides flux ratios for Johnson *B* and *V* bands (60 ± 20 and 130 ± 80 , respectively). Using the *H*- and *B*-band flux ratios, we are able to constrain the temperature of the companion star. We use NextGen stellar atmospheres (Hauschildt et al. 1999) restricted to the bandpasses with the size and temperature of the primary star to determine the secondary star’s effective temperature ($T_{\text{eff},B} = 6000^{+400}_{-300}$ K), radius ($R_B = 1.0 \pm 0.1 M_\odot$), luminosity ($L_B = 1.3 \pm 0.2 L_\odot$), and surface gravity ($\log g_B = 4.43 \pm 0.09$ (cm/s²)).

To model the observed ellipsoidal variations, we used the light-curve-fitting software package Eclipsing Light Curve (ELC; Orosz & Hauschildt 2000). ELC accurately

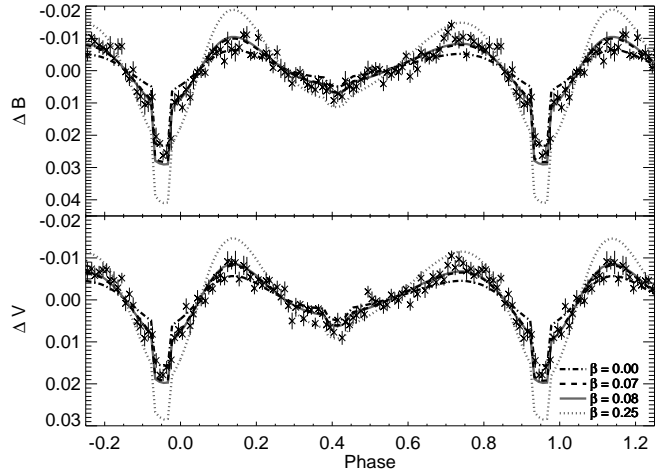


FIG. 5.— Differential folded and binned light curves of *o* Dra for *B* and *V* magnitudes plotted with error bars from the binning. Each data point is an average of data points spanning 0.01 in phase from the complete light curve folded on the orbital period. The quasi-sinusoidal signature of the averaged light curve is due to ellipsoidal variations caused by the primary star partially filling its Roche lobe potential. The lines represent the ELC models for ellipsoidal variations with the gravity darkening coefficient $\beta = 0.00, 0.07, 0.08$, and 0.25 , where $\beta = 0.07 \pm 0.03$ is the best fit to the binned light curves.

accounts for the star’s ellipsoidal shape which changes as the companion star moves along its eccentric orbit. We begin by modeling the light curves with no free parameters. We assume that the orbital and rotational axes are aligned ($i_{\text{orb}} = i_{\text{rot}}$, $P_{\text{rot}} = 79$ days), although our results are not sensitive to the assumed P_{rot} . We assume gravity darkening to be $\beta = 0.08$ (Lucy 1967). The ellipsoidal variations from the modeled light curves agree remarkably well with the observed light curve of *o* Dra confirming that the coherent quasi-sinusoidal signature is due to ellipsoidal variations (see Figure 5).

The long-term variations, ellipsoidal variations, and eclipses account for much of the large changes in the light curves, suggesting that the previously identified starspots (e.g., Hall & Persinger 1986; Strassmeier et al. 1989) were instead observations of a combination of these effects. Additionally, the absorption lines of the NOT spectra do not show clear evidence of rotationally-modulated temperatures due to starspots (see Figure 6).

However, weak spot signatures are occasionally still visually present after removing the eclipse and ellipsoidal variation model from the observed light curve. To determine a rotational period based on the spot signature, we perform a power spectrum analysis in which we sampled the light curve on a grid of one-day spacing (inserting 0.0 on days without data). We found the strongest signature comes from a period of $P_{\text{rot}} = 75$ days (see Figure 7), slightly smaller than the estimated 79-day period based upon $v \sin i$. While $P_{\text{rot}} = 75$ days is within 2σ from the spectroscopically determined rotation period, this small difference could be attributed to differential rotation, often seen with RS CVn stars (Strassmeier 2009).

Because the starspots are relatively weak, they do not strongly contaminate the phase-averaged light curve of *o* Dra, providing an opportunity for precision analysis. Using ELC, we measured the level of gravity darkening by modeling the system with no free parameters ex-

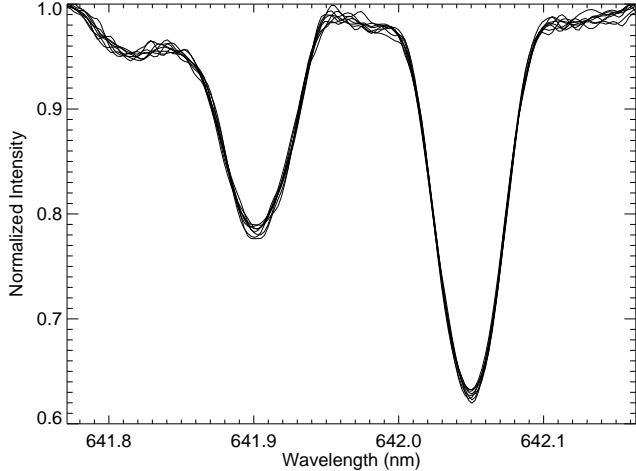


FIG. 6.— Portion of the *o* Dra spectrum containing two Fe I (6419 and 6421 Å) lines. Eight spectra are over-plotted spanning JD 2012 April 17 – August 15, approximately two rotation periods. Starspots moving across the stellar surface will manifest as features moving through some absorption lines. While the lines deviate from Gaussian profiles, throughout the rotation of *o* Dra, the absorption line cores do not vary in a periodic way, suggesting a featureless surface.

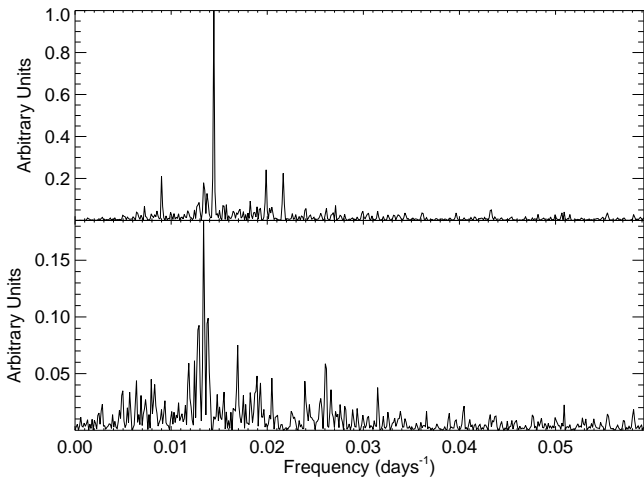


FIG. 7.— Power spectrum of the Johnson *B* light curve of *o* Dra. In the top panel, power spectrum of the *B* light curve with the long-term trend removed shows a peak at half the orbital period (69.2 days), consistent with the signature of ellipsoidal variations. In the bottom panel, the power spectrum of the *B* light curve with the long-term trend, eclipses, and ellipsoidal variations removed shows a peak at 75 days.

cept the gravity darkening coefficient, β from $T_{\text{eff}} \propto g^\beta$ (von Zeipel 1924). We found that the best-fit gravity darkening coefficient for *o* Dra is $\beta = 0.07 \pm 0.03$ (errors from bootstrapping over observational seasons), similar to recent findings of Djurašević et al. (2006, $\beta = 0.06 \pm 0.01$) and Roettenbacher et al. (2015, $\beta < 0.1$). These measurements are consistent with the canonical value $\beta \sim 0.08$ from Lucy (1967), but differs from an alternative value $\beta \sim 0.21$ from Espinosa Lara & Rieutord (2012).

5. HERTZSPRUNG-RUSSELL DIAGRAM AND EVOLUTIONARY HISTORY

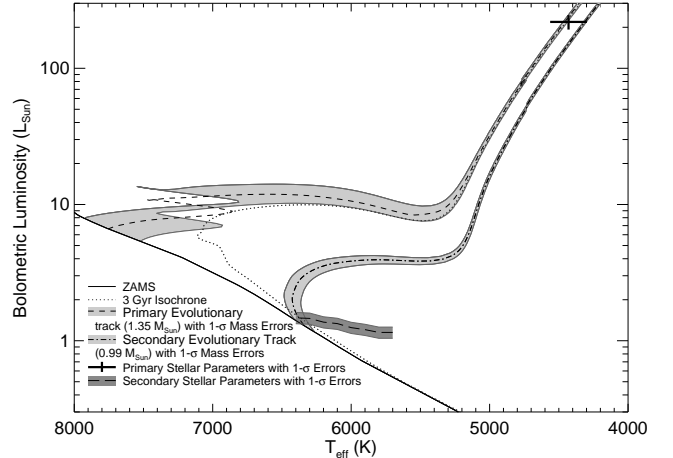


FIG. 8.— H-R diagram for *o* Dra. The dashed and dot-dashed lines are the main sequence and post-main sequence evolutionary tracks for $1.35 M_\odot$ and $0.99 M_\odot$ stars with $[Fe/H] \sim -0.5$, respectively (Dotter et al. 2008). The gray regions represent our $1-\sigma$ mass errors with the solid black line representing the zero age main sequence. The dotted line is a 3 Gyr isochrone (PHOENIX; Dotter et al. 2008). The measured location of the primary with $1-\sigma$ errors is indicated by the plus sign. The companion location is indicated with the long-dashed line (with $1-\sigma$ errors in luminosity).

To understand why *o* Dra has $P_{\text{rot}} < P_{\text{orb}}$, we investigate the evolution of the present stellar components. We plot the location of the components of *o* Dra on an H-R diagram (see Figure 8) using our measured stellar parameters determined from our orbit and flux ratios. We include the zero-age main sequence and Dartmouth stellar evolutionary tracks ($Fe/H = -0.5$, $\alpha/Fe = 0.0$, PHOENIX-based models, Dotter et al. 2008) for interpolated model masses ($M_{A,\text{model}} = 1.35 \pm 0.05 M_\odot$, $M_{B,\text{model}} = 0.99 \pm 0.02 M_\odot$).

Our primary star detection falls on the $1.35 M_\odot$ evolutionary track with an estimated temperature of 4430 ± 130 K (Christian & Janes 1977; Głęboczi & Stawikowski 1977; Rutter & Schrijver 1987; Głęboczi & Stawikowski 1988; McWilliam 1990; Luck 1991; Pourbaix & Boffin 2003; Böhm-Vitense 2004; Massarotti et al. 2008; Soubiran et al. 2010; McDonald et al. 2012). The detection of the secondary with $1-\sigma$ errors cross the main sequence of the expected evolutionary track, but at the upper limit of our temperature range ($T_{\text{eff},B} = 6000^{+400}_{-300}$ K). Our system age estimate most strongly depends upon the mass of the primary star; for the primary mass ($M_{A,\text{model}} = 1.35 \pm 0.05 M_\odot$), we determine an age of the system of 3.0 ∓ 0.5 Gyr.

We can use our knowledge of the evolutionary state of *o* Dra to investigate three possible explanations why the rotational period is faster than its orbital period. First, we conclude that the star could not have evolved right off of the main sequence. The rotational velocity is more rapid than expected ($\sim 3 \text{ km s}^{-1}$) for the evolution of a $1.35 M_\odot$, early F main sequence star (based upon initial rotational periods of ~ 2 days and main-sequence radius of $\sim 2 R_\odot$; Nielsen et al. 2013; Boyajian et al. 2012). Another component of the system must have imparted some angular momentum.

Second, secondary stars can spin-up primary stars faster than the orbital period in the case of eccentric orbits. Pseudosynchronous orbits are those that have the rotation of the star synchronized with the periastron passage of the secondary star (Hut 1981). *o* Dra has a predicted pseudosynchronous rotation period of $P_{\text{ps}} = 123.3 \pm 2.3$ days (Hall 1986), which is much longer than our observed rotational period. Thus, the known companion of *o* Dra could not have spun up the system to its current rotational period.

Third, a now-unseen companion could have spun-up the primary star. Because the secondary star has a mass of $M_{\text{B}} = 0.99 \pm 0.02 M_{\odot}$, the two objects that merged would have to have a significant difference in mass, otherwise the secondary star would be more evolved than the primary. With the primary and secondary stars falling on the same isochrone, the component that merged into the primary must have been only a small fraction of primary mass so as to not significantly affect its evolution. In order to be consistent with rotational velocity observations, sufficient angular momentum would need to be imparted by the merging component to spin-up the $\sim 1.04 M_{\odot}$ convective envelope of the $1.35 M_{\odot}$ primary star¹. Unfortunately, the rotation period of the star when the companion was engulfed is unknown and the primary star could have since slowed. While we cannot accurately estimate the mass of the consumed companion, we find from angular momentum arguments that the companion could range in mass from a giant planet to a low-mass star. If a low-mass companion were initially present in the system at 0.1 AU, it would be dynamically stable with the system's stellar components on the timescale of the system age, 3 Gyr, but would be engulfed by the primary star as the evolving stellar radius approached the companion's orbital radius (cf. David et al. 2003).

6. CONCLUSIONS

In this work, we have made the first visual detections of the secondary star of *o* Dra using interferometric observations. The *H*-band primary-to-secondary flux ratio is 370 ± 40 , the highest confirmed flux ratio for a binary detected with long-baseline optical interferometry. With the astrometry and radial velocity data for both stars, we establish the first full three-dimensional orbit to determine orbital and stellar parameters.

By folding and binning photometric data, we have shown evidence of ellipsoidal variations, gravitational distortions of the primary star caused by the close companion. The observed light curves are nearly identical to light curve models generated only from stellar and orbital parameters leading to the conclusion that the primary star has ellipsoidal variations, as opposed to long-lived starspots or active longitudes. After removing the model light curve, we observe only weak signs of rotationally-modulated starspots. Additionally, there could be poten-

tially active regions (e.g., axisymmetric spot structures and polar spots) that affect the stellar flux over longer periods of time with a global brightening or dimming. The folded, binned light curve also shows primary and secondary eclipses, which provide flux ratios to help constrain the stellar parameters of the secondary star.

Our new, high-precision orbital elements along with the folded light curve also allow for a measurement of gravity darkening. We find that $\beta = 0.07 \pm 0.03$, a value of gravity darkening consistent with conventional theory (Lucy 1967) and previous results (Djurašević et al. 2006; Roettenbacher et al. 2015).

We have established that the primary star's rapid rotation period could be due to the transfer of angular momentum from a nearby companion. Specifically, a low-mass companion in a 0.1 AU orbit would impart sufficient angular momentum to spin-up the outer stellar layers before being engulfed as the star ascended the giant branch while not dramatically altering the stellar evolution.

In this series of papers, we have demonstrated that precision interferometry at CHARA is capable of detecting the faint main-sequence companions of bright RS CVn primary stars. We are currently processing new data for another close, bright RS CVn system with the intention to publish these results in a follow-up paper.

ACKNOWLEDGEMENTS

We thank F. C. Adams, J. A. Orosz, D. Pourbaix, and M. Rieutord for their help and comments, as well as L. Boyd of Fairborn Observatory for his support of the photometric observations. The interferometric data in this paper were obtained at the CHARA Array, funded by the National Science Foundation through NSF grants AST-0908253 and AST-1211129, and by Georgia State University through the College of Arts and Sciences. The MIRC instrument at the CHARA Array was funded by the University of Michigan. NSF grant 1039522 from the Major Research Instrumentation Program, awarded to Tennessee State University, made extracting the secondary velocities possible. Astronomy at Tennessee State University is supported by the state of Tennessee through its Centers of Excellence program. The APT program was supported by NASA, NSF, Tennessee State University, and the Centers of Excellence Program. Nordic Optical Telescope is operated on the island of La Palma jointly by Denmark, Finland, Iceland, Norway, and Sweden, in the Spanish Observatorio del Roque de los Muchachos of the Instituto de Astrofísica de Canarias. R.M.R. would like to acknowledge support from the NASA Harriet G. Jenkins Pre-Doctoral Fellowship and a Sigma Xi Grant-in-Aid of Research. J.D.M. and R.M.R. acknowledge support of NSF grant AST-1108963. This research has made use of the SIMBAD database, operated at CDS, Strasbourg, France and the Jean-Marie Mariotti Center SearchCal service² co-developed by FIZEAU and LAOG/IPAG, and of CDS Astronomical Databases SIMBAD and VIZIER³.

¹ The mass of the convective envelope was determined using EZ-Web, <http://www.astro.wisc.edu/~simtownsend/static.php?ref=e-z-web>, R. H. D. Townsend's Web-browser interface of the Evolve ZAMS

evolution code (Paxton 2004)

² Available at <http://www.jmmc.fr/searchcal>

³ Available at <http://cdsweb.u-strasbg.fr/>

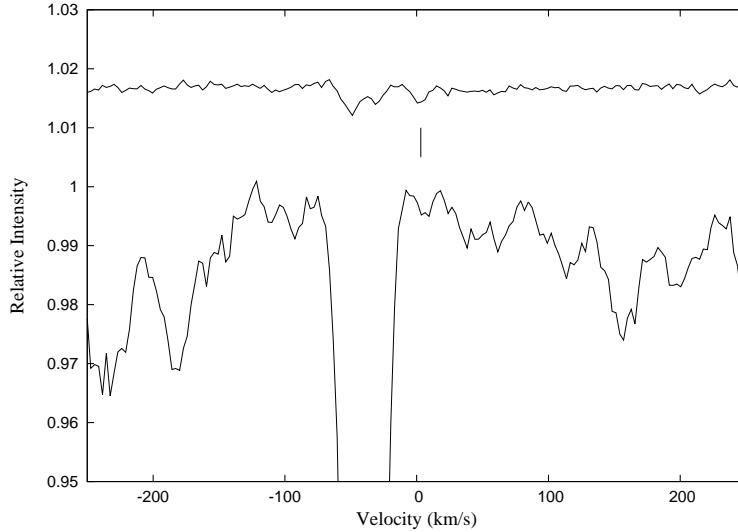


FIG. 9.— From a Fairborn Observatory spectrum of *o* Dra, the lower solid line is the average profile of the components summed over 168 spectral regions. The upper line, arbitrarily vertically shifted, is the remainder after the average region around the primary component from all useful Fairborn spectra has been removed from the lower line. The position of the secondary is indicated by a tick mark below the summed residual spectrum.

TABLE 7
o DRA ORBITAL PARAMETERS FROM RADIAL VELOCITY CURVES

Parameter	Massarotti et al. (2008)/CfA	AST/TSU
orbital period, P_{orb} (days)	138.45 ± 0.03	138.46 ± 0.01
center of mass velocity, γ (km s^{-1})	-20.8 ± 0.3	-20.87 ± 0.02
semi-amplitude, primary, K_A (km s^{-1})	23.48 ± 0.31	23.37 ± 0.03
semi-amplitude, secondary, K_B (km s^{-1})		31.86 ± 0.42
eccentricity, e	0.18 ± 0.02	0.154 ± 0.001
time of periastron passage, T (HJD)	2454982 ± 2	2455812.8 ± 0.2
longitude of periastron, ω_A ($^\circ$)	292 ± 5	290.7 ± 0.4
$M_A \sin^3 i$ (M_\odot)		1.34 ± 0.04
$M_B \sin^3 i$ (M_\odot)		0.99 ± 0.01
$a_A \sin i$ (10^6 km)		43.97 ± 0.05
$a_B \sin i$ (10^6 km)		59.92 ± 0.79
$a \sin i$ (R_\odot)	63.2 ± 0.9	
mass function, $f(M) = (M_B \sin i)^3 / (M_A + M_B)^2$	0.177 ± 0.007	
RMS velocity residuals, σ_A (km s^{-1})	0.39	0.16
RMS velocity residuals, σ_B (km s^{-1})		1.5

APPENDIX

A. AST RADIAL VELOCITIES

The secondary lines of *o* Dra were not obvious in the initial measurements of our individual AST spectra. Thus, similar to the method used by Fekel et al. (2015), we subtracted the spectrum of the primary, which was obtained by averaging our spectra, appropriately shifted so that all the primary lines from spectrum to spectrum were aligned. This subtraction resulted in a very weak average summed profile of the lines in the residual spectra corresponding to the secondary component (Figure 9). A Gaussian function was fitted to the very weak average secondary component to obtain its radial velocity. Because of the extreme weakness of the secondary lines and variable signal-to-noise ratio of the various spectra, most of the residual AST spectra did not produce measurable features of the secondary.

For the primary we determined a $v \sin i$ value of 15.6 ± 1.0 km s^{-1} , which is in good agreement with the value of 16.0 ± 0.5 km s^{-1} from the NOT spectra. The equivalent width ratio of the average component lines, A/B, which corresponds to the continuum intensity ratio, was measured in several AST spectra that had the highest signal-to-noise ratios. We find a ratio of 128 ± 4 at a mean wavelength of about 6000 Å, a value that is similar to the V band flux ratio of 130 found from the photometry.

The parameters from the AST double-lined spectroscopic orbit and the combined Massarotti et al. (2008)/CfA orbits are presented in Table 7.

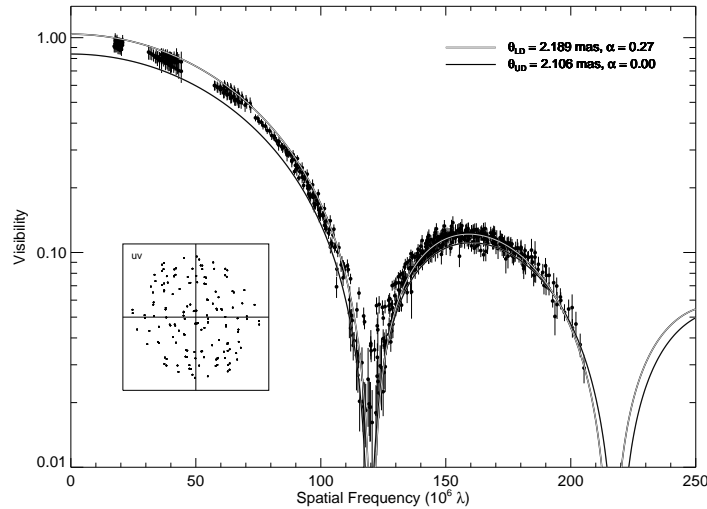


FIG. 10.— Visibility curve of the 2012 Jun 18 observations of *o* Dra with CHARA/MIRC. The observed visibility curve is plotted in black with 1σ error bars. The best-fit model from fitting for the companion is overplotted in as the black line ($\theta_{UD} = 2.106$ mas, $V(0) = 0.839$, $\alpha = 0.00$). The white line is our limb-darkened model ($\theta_{LD} = 2.189$ mas, $V(0) = 1.038$, $\alpha = 0.27$). The inset is the uv -coverage on the night of observation.

B. INTERFEROMETRIC OBSERVABLES

In Figures 10 - 13, we present a sample comparison of the calibrated *o* Dra data from 2012 Jun 18 and the best-fit detection of the companion from our χ^2 -space fit.

REFERENCES

- Basri, G., Laurent, R. & Walter, F. M. 1985, *ApJ*, 298, 761
 Basri, G. 1987, *ApJ*, 316, 377
 Berdyugina, S. V. 2005, *LRSP*, 2, 8
 Böhm-Vitense, E. 2004, *AJ*, 128, 2436
 Bonneau, D., Clausse, J.-M., Delfosse, X., et al. 2006, *A&A*, 456, 789
 Boyajian, T. S., McAlister, H. A., van Belle, G., et al. 2012, *ApJ*, 746, 101
 ten Brummelaar, T. A., McAlister, H. A., Ridgway, S. T., et al. 2005, *ApJ*, 628, 453
 Castelli, F. & Kurucz, R. L. 2004, *Modelling of Stellar Atmospheres*, ed. N. Piskunov et al., IAU Symp., 210 [arXiv:astro-ph/0405087]
 Che, X., Monnier, J. D., Zhao, M., et al. 2011, *ApJ*, 732, 68
 Christian, C. A. & Janes, K. A. 1977, *PASP*, 89, 415
 Claret, A. 2009, *A&A*, 507, 377
 David, E.-M., Quintana, E. V., Fatuzzo, M., & Adams, F. C. 2003, *PASP*, 115, 825
 Djurašević, G., Rovithis-Livaniou, H., Rovithis, P., Georgiades, N., Erkapic, S., Pavlović 2006, *A&A*, 445, 291
 Dotter, A., Chaboyer, B., Javremović, D. et al. 2008, *ApJS*, 178, 89
 ESA. 1997, *The Hipparcos and Tycho Catalogues* (ESA SP-1200)
 Espinosa Lara, F. & Rieutord, M. 2012, *A&A*, 547, 32
 Fekel, F. C., Henry, G. W., & Lewis, C. 2005, *AJ*, 130, 794
 Fekel, F. C., Tomkin, J., & Williamson, M. H. 2009, *AJ*, 137, 3900
 Fekel, F. C., Williamson, M. H., Muterspaugh, M. W., Pourbaix, D., Willmarth, D., & Tomkin, J. 2015, *AJ*, 149, 63
 Gallenne, A., Mérand, A., Kervella, P., Monnier, J. D., Schaefer, G. H., et al. 2015, *A&A*, 579, 68
 Głębcki, R. & Stawikowski, A. 1977, *Acta Astron.*, 27, 225
 Głębcki, R. & Stawikowski, A. 1988, *A&A*, 189, 199
 Gurzadyan, G. A. & Cholakyan, V. G. 1995, *Ap&SS*, 229, 185
 Hall, D. S. 1976, in *ASSL Vol. 60: IAU Colloq. 29: Multiple Periodic Variable Stars*, ed. W. S. Fitch (Dordrecht: Reidel), 287
 Hall, D. S. 1986, *ApJ*, 309, L83
 Hall, D. S. & Persinger, W. T. 1986, in *LNP Vol. 254: Cool Stars, Stellar Systems and the Sun*, eds. M. Zeilik & D. M. Gibson, 88
 Hauschildt, P. H., Allard, F., Ferguson, J., Baron, E., & Alexander, D. R. 1999, *ApJ*, 525, 871
 Heintz, W. D. 1978, *Double Stars* (Dordrecht: Reidel)
 Henry, G. W. 1999, *PASP*, 111, 845
 Herbig, G. H. & Spalding, J. Jr. 1955, *ApJ*, 121, 118
 Hut, P. 1981, *A&A*, 99, 126
 Koch, R. H. & Hrivnak, B. J. 1981, *AJ*, 86, 438
 van Leeuwen, F. 2007, *A&A*, 474, 653
 Luck, R. E. 1991, *ApJS*, 75, 579
 Lucy, L. B. 1967, *Zs. Ap.*, 65, 89
 Lucy, L. B. & Sweeney, M. A. 1971, *AJ*, 76, 544
 Massarotti, A., Latham, D. W., Stefanik, R., & Fogel, J. 2008, *AJ*, 135, 209
 Mayor, M. & Mermilliod, J.-C. 1984, *Observational Tests of the Stellar Evolution Theory*, ed. A. Maeder, A. Renzini, in *IAU Symp.*, 105, 411
 Mazeh, T. 2008, *EAS*, 29, 1
 McDonald, I., Zijlstra, A. A., Boyer, M. L. 2012, *MNRAS*, 427, 343
 McWilliam, A. 1990, *ApJS*, 74, 1075
 Monnier, J. D., Berger, J., Millan-Gabet, R., & ten Brummelaar, T. A. 2004, *Proc. SPIE*, 5491, 1370
 Monnier, J. D., Pedretti, E., Thureau, N., et al. 2006, *Proc. SPIE*, 6268, 62681
 Monnier, J. D. 2007, *New Astron. Rev.*, 51, 604
 Monnier, J. D., Che, X., Zhao, M., et al. 2012, *ApJL*, 761, L3
 Nelson, E. R. & Zeilik, M. 1990, *ApJ*, 349, 163
 Nielsen, M. B., Gizon, L., Schunker, H., & Karoff, C. 2013, *Progress in Physics of the Sun and Stars: A New Era in Helio- and Asteroseismology*, ed. H. Shibahashi & A. E. Lynas-Gray, in *ASPC*, 479, 137
 Orosz, J. A. & Hauschildt, P. H. 2000, *A&A*, 364, 265
 Paxton, B. 2004, *PASP*, 116, 699
 Pourbaix, D. & Boffin, H. M. J. 2003, *A&A*, 398, 1163
 Roettenbacher, R. M., Monnier, J. D., Henry, G. W., Fekel, F. C., Williamson, M. H. et al. 2015, 807, 23
 Rutter, R. G. M. & Schrijver, C. J. 1987, *A&A*, 177, 155
 Schröder, K.-P. & Connon Smith, R. 2008, *MNRAS*, 386, 155
 Simon, T. & Fekel, F. C., Jr. 1987, *ApJ*, 316, 434
 Soubiran, C., Le Campion, J.-F., Cayrel de Strobel, G., & Caillo, A. 2010, *A&A*, 515, 111
 Stefanik, R. P., Latham, D. W., & Torres, G. 1999, in *Precise Stellar Radial Velocities*, *ASP Conf. Series* 185, IAU Colloq. 17: Eds. J. B. Hearnshaw & C. D. Scarfe, 354

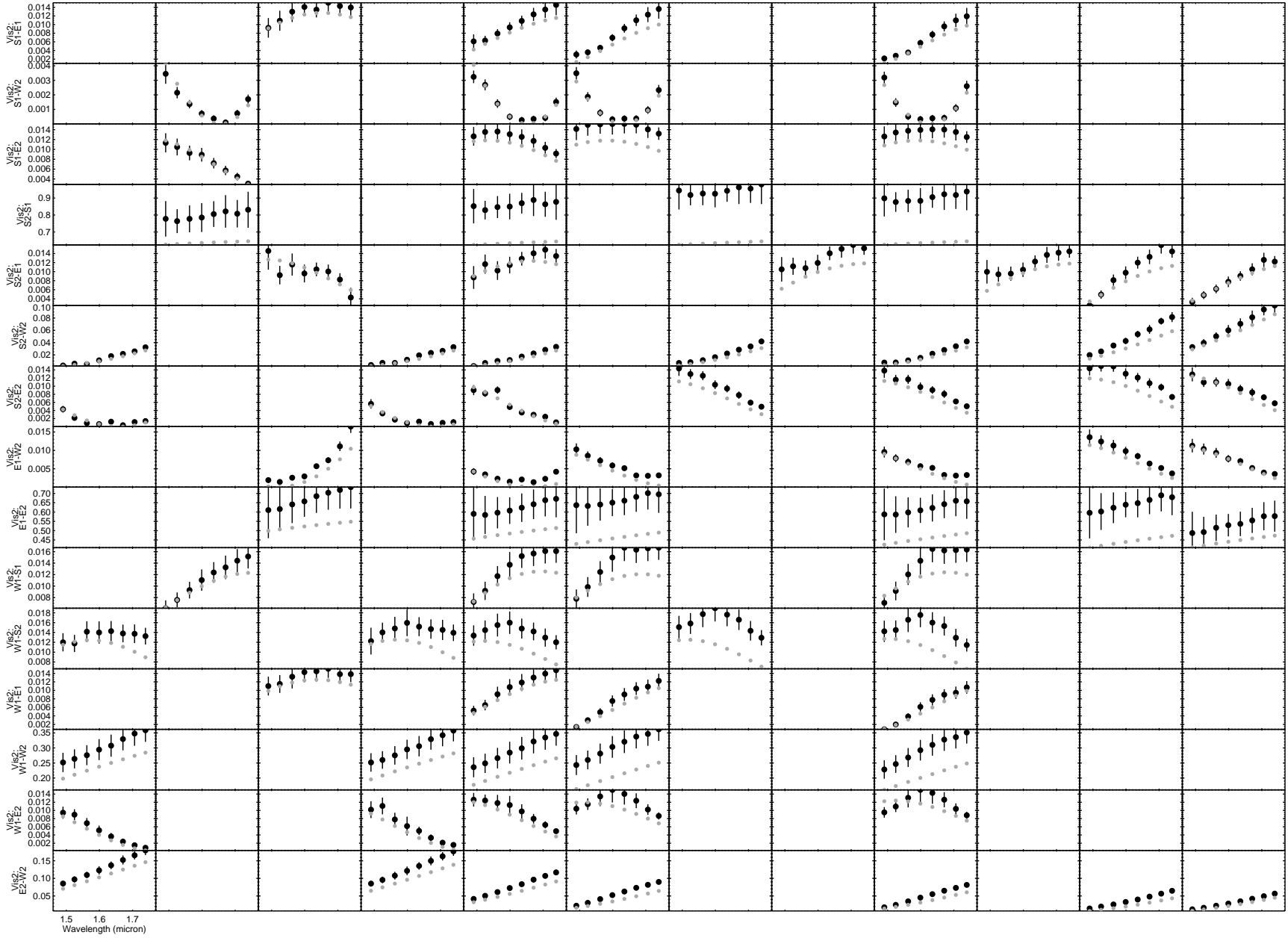


FIG. 11.— Squared visibilities of the 2012 Jun 18 observations of σ Dra with CHARA/MIRC. Each block of observations represents a temporal block of observations. The data and model are plotted as in Figure 10.

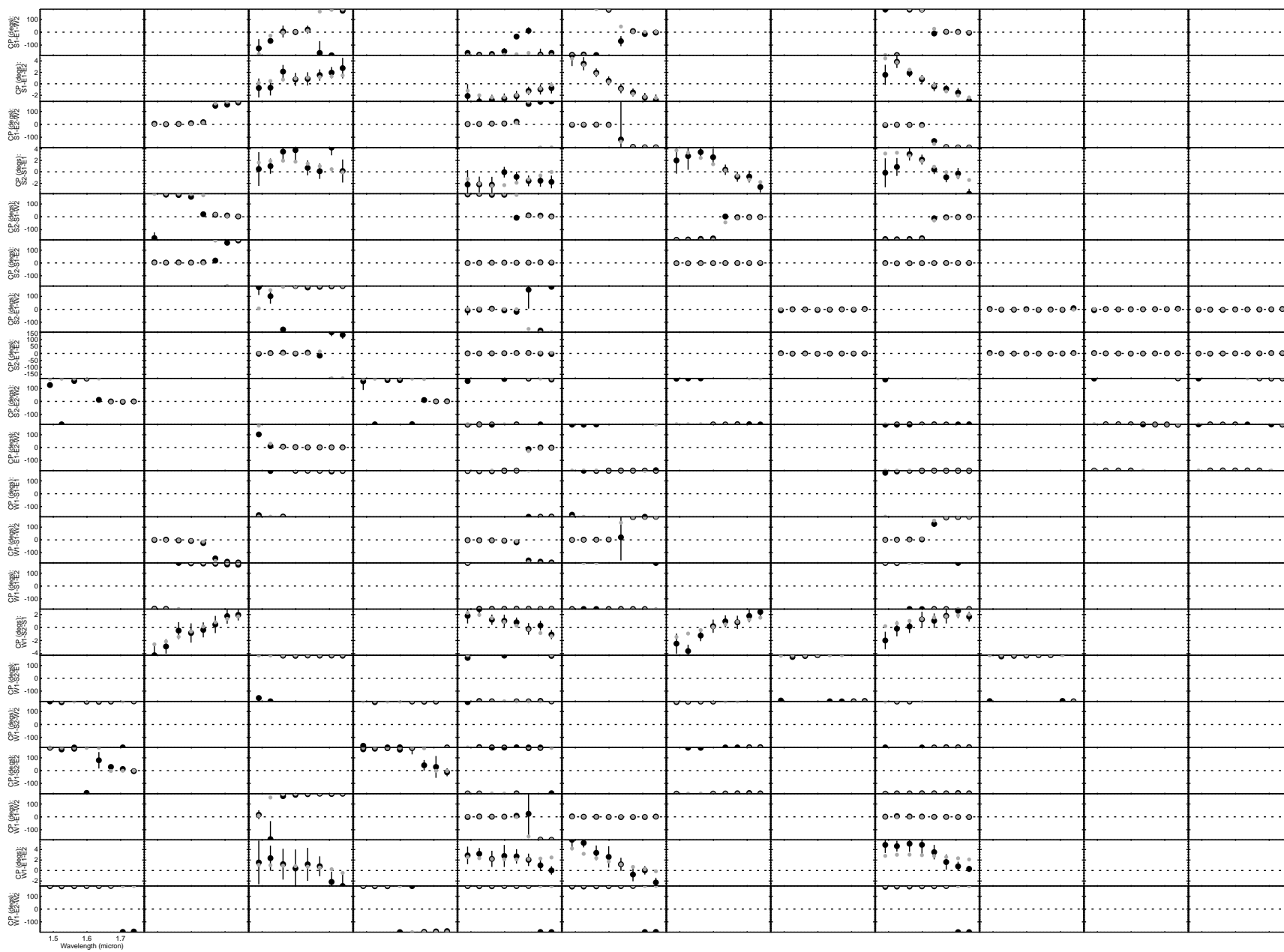


FIG. 12.— Closure phases of the 2012 Jun 18 observations of *o* Dra with CHARA/MIRC plotted as in Figure 11.

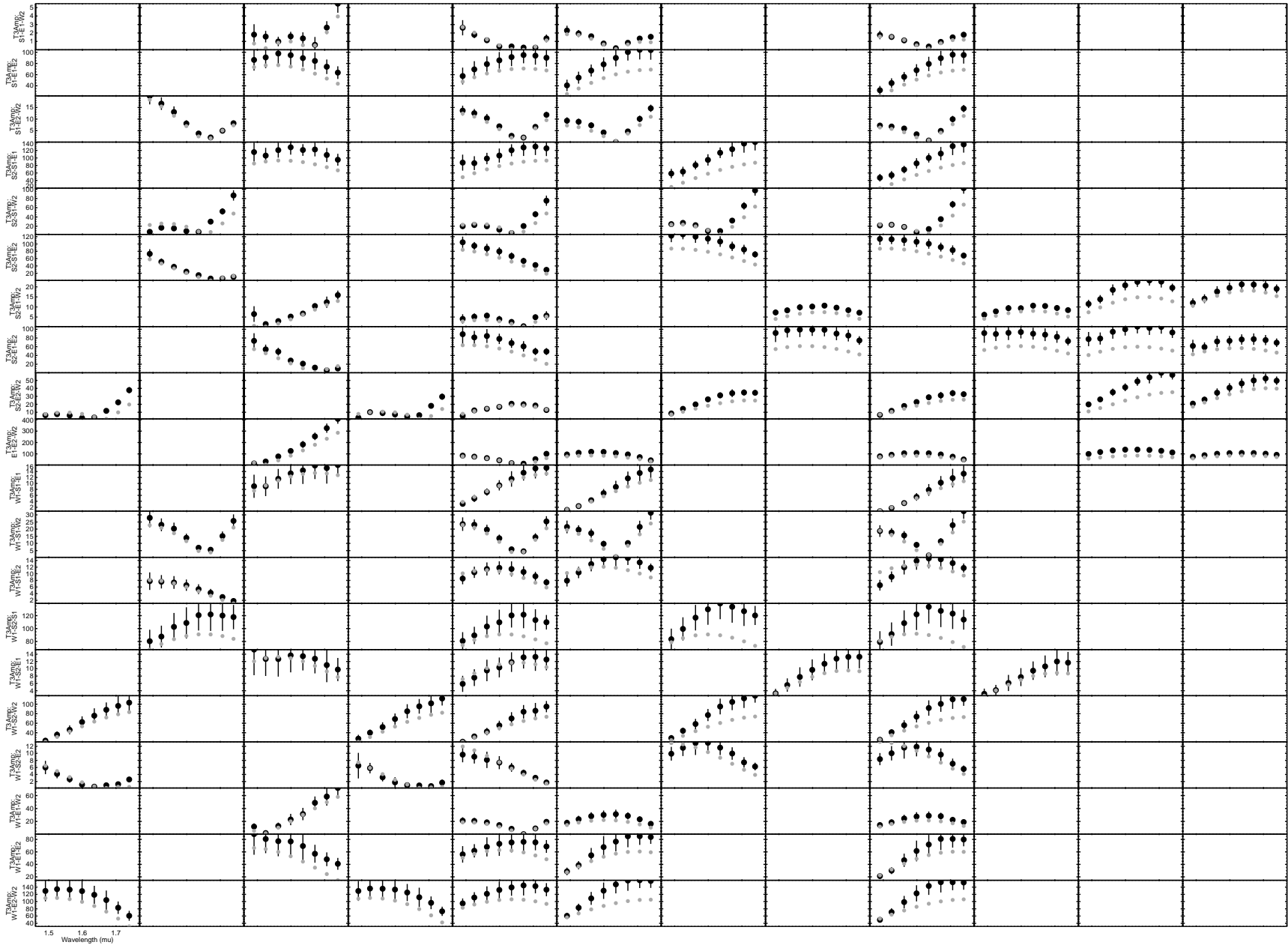


FIG. 13.— Triple amplitudes (multiplied by 10^4 for clarity) of the 2012 Jun 18 observations of *o* Dra with CHARA/MIRC plotted as in Figure 11.

- Strassmeier, K. G. 2009, *A&ARv*, 17, 251
Strassmeier, K. G., Hall, D. S., Eaton, J. A., et al. 1988, *A&A*, 192, 135
Strassmeier, K. G., Hall, D. S., Boyd, L. J., & Genet, R. M. 1989, *ApJS*, 69, 141
Walter, K. 1949, *Nature*, 164, 1129
Walter, F. M. 1985, *PASP*, 97, 643
White, T. R., Huber, D., Maestro, V., Bedding, T. R., Ireland, M. J. et al. 2013, *MNRAS*, 433, 1262
Young, R. K. 1921, *JRASC*, 15, 161
Young, A. & Koniges, A. 1977, *ApJ*, 211, 836
Zahn, J.-P. 1977, *A&A*, 57, 383
Zahn, J.-P. & Bouchet, L. 1989, *A&A*, 223, 112
von Zeipel, H. 1924, *MNRAS*, 84, 655
Zhao, M., Monnier, J. D., Pedretti, E., et al. 2009, *ApJ*, 701, 209